Mechanism of the Interaction of β_2-Glycoprotein I with Negatively Charged Phospholipid Membranes†

Michal Hammel,‡ Robert Schwarzenbacher,‡,§ Anna Gries,|| Gerhard M. Kostner,⊥ Peter Laggner,‡ and Ruth Prassl*,‡

Institute of Biophysics and X-ray Structure Research of the Austrian Academy of Sciences, Schmiedlstrasse 6, A-8042 Graz, Austria, Institute of Physiology, University of Graz, Harrachgasse 21, A-8010 Graz, Austria, and Institute of Medical Biochemistry, University of Graz, Harrachgasse 21, A-8010 Graz, Austria

Received July 10, 2001; Revised Manuscript Received August 30, 2001

ABSTRACT: In an attempt to understand the multifunctional involvement of β_2-glycoprotein I (β_2GPI) in autoimmune diseases, thrombosis, atherosclerosis, and inflammatory processes, substantial interest is focused on the interaction of β_2GPI with negatively charged ligands, in particular, with acidic phospholipids. In this study, unilamellar vesicles composed of cardiolipin were used as in vitro membrane system to test and further refine a model of interaction based on the crystal structure of β_2GPI. The data suggest that β_2GPI anchors to the membrane surface with its hydrophobic loop adjacent to the positively charged lysine rich region in domain V. Subsequently, β_2GPI penetrates the membrane interfacial headgroup region as indicated by a restriction of the lipid side chain mobility, but without formation of a nonbilayer lipid phase. A structural rearrangement of β_2GPI upon lipid binding was detected by microcalorimetry and may result in the exposure of cryptic epitopes located in the complement control protein domains. This lipid-dependent conformational change may induce oligomerization of β_2GPI and promote intermolecular associations. Thus, the aggregation tendency of β_2GPI may serve as the basis for the formation of a molecular link between cells but may also be an essential feature for binding of autoantibodies and hence determine the role of β_2GPI in autoimmune diseases.

β_2-Glycoprotein I (β_2GPI),[1] also designated apolipoprotein H, is an abundant human plasma glycoprotein that is found in both free and lipoprotein-associated forms (*1*, *2*). Although the physiological role of β_2GPI in biological fluids is unknown, in vitro studies have shown that β_2GPI plays a triggering role in the blood coagulation cascade (*3*), in platelet aggregation (*4*−*7*), and in the course of thrombolytic diseases (*3*, *8*). β_2GPI preferentially binds to surfaces carrying negative charges. Prominent candidates for interaction in vivo are cell membranes or endothelial cells (*9*, *10*) containing acidic phospholipids such as cardiolipin or phosphatidylserine. In the course of apoptotic or necrotic cell death, anionic phospholipids which are normally located in the inner side of the membrane may become surface-exposed and act as a target for β_2GPI. Hence, β_2GPI may trigger the recognition of apoptotic cells by inflammatory macrophages (*11*) and mediate the clearance of liposomal particles by phagocytic cells (*12*, *13*). Likewise, such associations of β_2-GPI with lipids are considered to act as antigens for antiphospholipid autoantibodies (aPLAs) associated with clinical events such as systemic lupus erythematosus or antiphospholipid syndrome (*14*, *15*). The structural basis for the mechanism of binding of β_2GPI to lipid ligands, subsequent cell recognition, and the interaction with specific aPLAs is still unclear. Structural rearrangement of the phospholipid vesicles (*5*), conformational changes of β_2GPI (*14*, *16*−*19*), and generation of specific protein clusters (*20*, *21*) are heavily discussed. This special issue will also be addressed in this study, proceeding from the three-dimensional X-ray crystal structure, which has been determined recently (*22*, *23*).

β_2GPI is a single-chain glycoprotein of 326 amino acid residues and consists of four complement control protein (CCP) modules and a distinct C-terminal domain V. From the crystal structure, it is known that the four CCP domains exhibit an elliptically shaped β-sandwich structure comprised of several antiparallel β-strands wrapped around a well-defined hydrophobic core containing one conserved tryptophan each. In contrast, domain V folds into a central β-spiral with two small helices and carries a distinct positive

† This work was supported by a grant from the Austrian Science Foundation (Project P13872-CHE) to R.P.

* To whom correspondence should be addressed: Institute of Biophysics and X-ray Structure Research of the Austrian Academy of Sciences, Schmiedlstr. 6, A-8042 Graz, Austria. Telephone: (+43)-316-4120-305. Fax: (+43)-316-4120-390. E-mail: ruth.prassl@oeaw.ac.at.

‡ Institute of Biophysics and X-ray Structure Research of the Austrian Academy of Sciences.

§ Present address: The Burnham Institute, 10901 N. Torrey Pines Rd., La Jolla, CA 92037.

|| Institute of Physiology, University of Graz.

⊥ Institute of Medical Biochemistry, University of Graz.

[1] Abbreviations: β_2GPI, β_2-glycoprotein I; aPLAs, antiphospholipid autoantibodies; CCP, complement control protein; DMPS, 1,2-dimyristoyl-*sn*-glycero-3-phosphatidylserine; DMPC, 1,2-dimyristoyl-*sn*-glycero-3-phosphatidylcholine; CL, bovine heart cardiolipin; LUV, large unilamellar vesicle; DSC, differential scanning calorimetry; T_m, melting transition temperature; ΔH_{cal}, calorimetric enthalpy; ΔH_{vH}, van't Hoff enthalpy; ESR, electron spin resonance; 5-CL, 1-(3-*sn*-phosphatidyl)-3-{1-acyl-2-[*n*-(4,4-dimethyloxazolidine-*N*-oxyl)stearoyl]glycero-3-phospho}-*sn*-glycerol; 12-CL, 1-(3-*sn*-phosphatidyl)-3-{1-acyl-2-[12-(4,4-dimethyloxazolidine-*N*-oxyl)stearoyl]glycero-3-phospho}-*sn*-glycerol; SD, standard deviation.

10.1021/bi0114372 CCC: $20.00 © 2001 American Chemical Society
Published on Web 11/02/2001

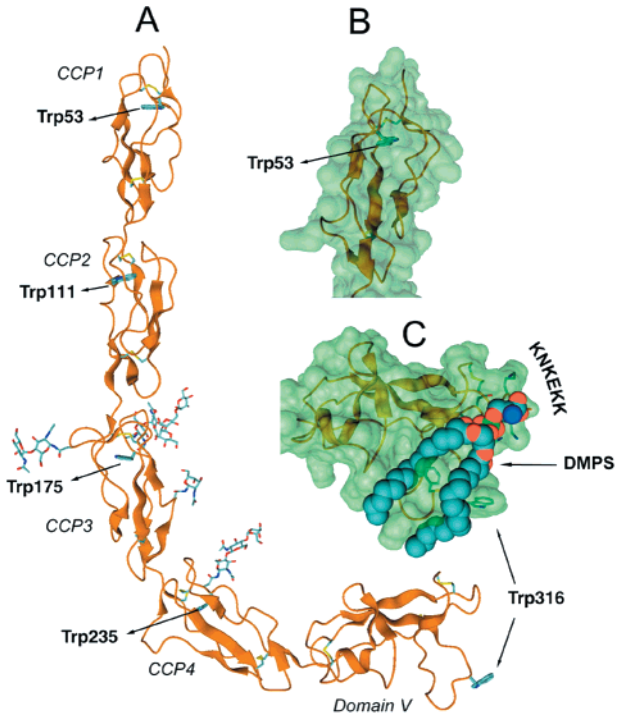

FIGURE 1: Structural model of β_2GPI and molecular modeling simulation of the lipid−protein interaction. (A) Ribbon diagram of β_2GPI derived from the X-ray crystal structure (*23*) (Protein Data Bank entry 1C1Z). The β-strands are shown in ochre. The disulfide bonds are shown in yellow. The four N-linked glycans and the five Trp residues are shown in an all-atom representation. (B) For a better illustration, a partial magnification of CCP1 as a representative for the four CPP domains is shown in a molecular surface presentation. It can be seen that the Trp residues located in CCP1−4 are buried in the interior of the protein backbone, whereas Trp316 in domain V is part of the surface-exposed hydrophobic loop. (C) A model of a putative association of a negatively charged phospholipid molecule (DMPS) with domain V residues 244−326. The simulation of the molecular model was derived from computer docking studies with the program DOCK (*32*). While domain V was kept fixed, the DMPS molecule was allowed to find its optimal position. The main chain atoms of the positively charged, lysine rich part (KNKEKK) are indicated.

charge in the proximity of a surface-exposed loop region comprising Trp316. On the basis of the hypothesis that domain V carries the lipid binding region within the sequence motif C^{281}KNKEKKC^{288}, we performed a computer-aided docking study to describe the putative association of an acidic lipid molecule to domain V (Figure 1). In addition to the lysine rich region, our model further outlines the involvement of the hydrophobic loop (LAWF) in binding processes. To obtain additional experimental evidence for this hypothesis, we applied fluorescence spectroscopy, taking advantage of the fact that β_2GPI contains five tryptophan residues, one in each domain (see Figure 1) which are, except for Trp316, embedded in the hydrophobic interior. Next, we addressed the question of whether the interaction of β_2GPI with phospholipids is accompanied by a rearrangement of the protein structure or if the main impact occurs on the phospholipid membrane side. Further, we aimed to investigate how deep the protein penetrates the lipid membrane and whether a nonbilayer or multilamellar phase is induced. Finally, the macroscopic effect of β_2GPI on vesicular solutions was viewed by turbidity measurements and light microscopy.

MATERIALS AND METHODS

Materials. 1,2-Dimyristoyl-*sn*-glycero-3-phosphatidylcholine (DMPC), bovine heart cardiolipin (CL), and monolysocardiolipin were purchased from Avanti Polar Lipids (Birmingham, AL). The purity of the lipids was tested by thin-layer chromatography using a $CHCl_3/CH_3OH/H_2O$ mixture (65:35:5, v/v) as the mobile phase. Spin-labeled stearic acids with the nitroxyl group either at C-5 or at C-12 and all other chemicals were obtained from Sigma (Vienna, Austria).

Protein. β_2GPI was isolated from citrated human plasma as described previously (*1*, *24*). The protein was purified by column chromatography, exhaustively dialyzed against Tris-HCl (pH 7.4), and finally dialyzed against NH_4HCO_3 before lyophilization. The preparation was virtually 100% pure as judged by SDS−polyacrylamide gel electrophoresis, where one single band with an apparent molecular mass of 55 kDa was seen. If not stated otherwise, the protein was dissolved in 50 mM Tris-HCl and 25 mM NaCl (pH 7.4) (briefly, Tris-HCl) immediately before use. The protein concentration was measured by the bicinchoninic acid assay (BCA assay, Pierce).

Preparation of Phospholipid Vesicles. DMPC was dissolved in a chloroform/methanol mixture (3:1, v/v) and CL in chloroform. A dry lipid film was prepared by evaporation of the organic solvent followed by storage under a high vacuum overnight. The lipid films were then resuspended in Tris-HCl and vortexed vigorously. The lipid suspensions were hydrated for approximately 2 h above the transition temperature. Large unilamellar vesicles (LUVs) were prepared by powered extrusion through 0.1 μm pore diameter polycarbonate filters (Nuclepore) in a LiposoFast pneumatic extruder (Avestin Inc., Ottawa, ON). The phospholipid concentration was determined by phosphate analysis according to the method of Bartlett (*25*). The lipid concentration was in all cases approximately 1 mg/mL, and the dispersions were used directly for the experiments.

Intrinsic Trp Fluorescence. Fluorescence experiments were carried out on a Perkin-Elmer LS-B50 fluorescence spectrophotometer using a 10 mm × 10 mm quartz fluorescence cuvette. For proteins containing both tyrosine and tryptophan residues, the latter may be excited selectively at 290−295 nm (*26*). Hence, the excitation wavelength chosen for all spectra was 292 nm with a slit width of 5 nm and an integration time of 0.05 s. The spectra were taken as the mean of 10 scans. The background intensity of the samples without protein was subtracted before determination of emission maxima and fluorescence intensities. Titration experiments were performed by pipetting different aliquots of LUVs suspended in Tris-HCl buffer into the cuvette containing β_2GPI (50 μg/mL, 1.1 μM) dissolved in the same buffer. The CL:β_2GPI molar ratio was in the range of 0−40. Alternatively, samples were prepared by mixing 750 μL of 2.2 μM β_2GPI solutions and 750 μL of CL vesicles with varying concentrations (CL:β_2GPI molar ratio in the range of 0−88). The temperature of the cuvette was maintained at 25 °C, and the measurements were taken after equilibration for 10 min.

For the analysis of emission-dependent membrane partitioning by means of fluorescence intensity, we used a quartz fluorescence cuvette (2 mm × 10 mm) oriented perpendicular to the excitation beam. The excitation wavelength was set

to 270 nm with a slit width of 10 nm and an integration time of 0.5 s. Cross-oriented polarizers (Em = 0°, Ex = 90°) were used to minimize the scattering background. As scattering light from vesicles, unlike light absorbed by an additional nonfluorescent substance, can still excite Trp fluorescence, it is not possible to correct for the attenuation caused by scattering using equations for the inner filter effect (*27*). Instead, an empirical correction using a tryptophan reference was applied (*28*). We used the intensity data from a nonpartitioning Trp zwitterion measured at similar scattering values [A_{470}] as in the case of CL/β_2GPI mixtures (see absorbance measurements). To approach this, varying CL concentrations were added to a 0.01 mM Trp solution in Tris-HCl containing 0.1 M Ca^{2+}. The corrected fluorescence intensity ($I^{\text{corrected}}[A_{470}]$) for each CL:$\beta_2$GPI ratio was determined according to

$$I^{\text{corrected}}[A_{470}] = I[A_{470}]\frac{I_{\text{Trp}}^{\text{buffer}}}{I_{\text{Trp}}[A_{470}]} \quad (1)$$

where $I_{\text{Trp}}^{\text{buffer}}$ and $I_{\text{Trp}}[A_{470}]$ are the fluorescence intensities in the emission maximum of the Trp reference in the absence and presence of CL, respectively. $I[A_{470}]$ is the uncorrected fluorescence intensity for the scattering values [A_{470}]. It is known that even low concentrations of Ca^{2+} induce a conversion of a lamellar to hexagonal phase in cardiolipin vesicles, visible as formation of milky turbid dispersions (*29*). These dispersions were used to calibrate the fluorescence signal of a Trp reference for the scattering values of the vesicles. Note the fluorescence measurements in the presence of β_2GPI were performed without Ca^{2+}.

Anisotropy. Anisotropy measurements were performed with a polarization accessory unit. Steady-state fluorescence anisotropy, *r*, was measured according to

$$r = (I_{||} - gI_{\perp})/(I_{||} + 2gI_{\perp}) \quad (2)$$

where $g = I_{\perp}/I_{||}$ and $I_{\perp}$ and $I_{||}$ are the perpendicular and parallel components of fluorescence polariziation, respectively, relative to the plane of polarization of the excitation beam. An excitation wavelength of 292 nm and an emission wavelength of 351 nm were used with a slit width of 15 nm and an integration time of 2.4 s. A mean number of 20 measurements were taken.

Acrylamide Quenching of Trp Fluorescence. Aliquots of a stock solution of 5 M acrylamide in Tris-HCl were added to a 1.1 μM solution of β_2GPI in the absence and presence of 20 mol of CL/mol of protein. The acrylamide concentration was varied in a range between 0.02 and 0.6 M. An excitation wavelength of 292 nm with a slit width of 5 nm and an integration time of 0.1 s was used. The fluorescence quenching data were analyzed by using the modified Stern−Volmer equation

$$I_0/(I_0 - I) = 1/f_a + 1/(f_a K_a[Q]) \quad (3)$$

where I and I_0 are the fluorescence intensities in the presence and absence of quencher, respectively, f_a is the fraction of initial fluorescence which is accessible to the quencher, K_a is the Stern−Volmer quenching constant of the accessible fraction, and [Q] is the quencher concentration. The measured fluorescence was corrected for the volume increase and the inner filter effect on the excitation beam caused by acrylamide ($\epsilon_{292} = 0.34\ M^{-1}\ cm^{-1}$) (*30*). The modified Stern−Volmer equation allows f_a and K_a to be determined graphically.

Differential Scanning Calorimetry (DSC). Calorimetric experiments were performed in a high-sensitivity adiabatic DASM-4 scanning microcalorimeter (Biobribor, Pushtchino, Russia) (*31*). Temperature scanning was carried out from 1 to 85 °C, all scans being performed with 10 mM Hepes buffer (pH 7.4) in the reference cell. The cells were maintained under a nitrogen pressure of ~250 kPa to avoid air bubble formation. DSC measurements on native β_2GPI were performed at two different protein concentrations [0.2 and 0.5 mg/mL in 10 mM Hepes buffer (pH 7.4)] and scan rates of 60 and 90 °C/h. The reversibility of unfolding was tested by repeated scans, and at least duplicates were run. Calorimetric measurements on complexes of CL vesicles and β_2-GPI were performed at a constant protein concentration of 0.5 mg/mL at lipid:protein molar ratios of 1 and 20 at a scan rate of 60 °C/h. Pure bovine heart cardiolipin showed no thermal transition in the range from 1 to 85 °C. DSC data were analyzed by first subtracting the corresponding buffer baseline and normalization to protein concentration. For the integration of the heat capacity, a cubic progress baseline for the native and heat-denatured state was defined. The transition temperature (T_m) was taken from the maximum in the peak position, and the transition enthalpy (ΔH_{cal}) was obtained from the area under the curve. The van't Hoff enthalpy (ΔH_{vH}) was calculated from the maximum in the heat capacity function, the calorimetric enthalpy, the gas constant, and the transition temperature by applying a non-two-state curve fitting function.

Electron Spin Resonance (ESR). Cardiolipin molecules spin-labeled at C-5 (5-CL) or C-12 (12-CL) of the *sn*-2′ chain were synthesized from monolysocardiolipin according to the method described by Cable et al. (*32*). Finally, the cardiolipin spin-label was taken from preparative TLC plates. Unlabeled and spin-labeled CL (molar ratio of 100:1) were codissolved in chloroform dried under a stream of nitrogen and subsequently under vacuum overnight. The dry lipid film was then dispersed in Tris-HCl or solutions of β_2GPI to yield a final concentration of 4 mM CL at lipid:protein molar ratios of 20:1 and 50:1. ESR spectra were recorded on an X-band ECS 106 spectrometer (Bruker, Rheinstetten, Germany) at 20 °C with a modulation amplitude of 1.2 G (p−p) and a sweep width of the static field of 100 G.

Small-Angle and Wide-Angle X-ray Diffraction (SWAXS). SWAXS experiments were performed on a modified Kratky compact camera (HECUS-MBraun, Graz, Austria) equipped with two linear one-dimensional position sensitive OED50M detectors (MBraun, Garching, Germany), a Ni-filtered (10 μm) beam-stop system, and an automatic data collection unit. The camera was operated at a rotating anode (RU-200B, Rigaku Denki) with Cu Kα radiation (wavelength of 1.542 Å). Samples were measured in a 1 mm diameter quartz capillary. The scattered X-ray intensities were evaluated as a function of a scattering angle 2θ and converted into reciprocal units with the relation $h = 4\pi/\lambda$ (sin 2θ). The data were corrected for slit collimation and background. The desmearing of data and transformation in real space in terms of their pair distance distribution function was performed with the program ITP (*33*). The concentration of CL vesicles

was 4 mM, and the concentration of β_2GPI was 0.2 mM, both in 10 mM Hepes buffer (pH 7.4). An exposure time of 3600 s was chosen to guarantee an appropriate signal-to-noise ratio.

Turbidity Measurements. Aggregation of CL vesicles caused by β_2GPI was monitored by measuring the absorbance at 470 nm (A_{470}) using a Beckman DU 640 spectrophotometer and cuvettes with an optical path of 1 cm. To 750 μL of a 2.2 μM β_2GPI solution in Tris-HCl was added 750 μL of CL vesicles of varying concentrations, as was done for fluorescence experiments, and the mixture was equilibrated for 10 min at room temperature before measurements were taken. The data were corrected for the background scattering of CL vesicles which was less than 5%. Subsequently, the samples were centrifuged at 15000*g* for 15 min in a Sigma 3K18 centrifuge (12110-H rotor) to separate CL LUVs−β_2-GPI aggregates from the unbound protein. The white precipitate at the bottom of the vial was collected and the supernatant analyzed for protein content (BCA assay).

Light Microscopic Images. Small droplets of sample were placed on microscopic slides and covered with thin glass coverslips. The samples were observed with bright field illumination in a Leica DM L microscope equipped with an oil immersion PL Fluotar semiapochromate 100×/1.30 objective. The images were viewed with a PC-connected video camera system. Shaken-only vesicles of CL and mixtures with β_2GPI in a concentration range from 1 to 200 lipid molecules per β_2GPI molecule were investigated at a constant CL concentration of 1 mM.

Molecular Modeling. A model of a putative association of a negatively charged phospholipid (DMPS) to domain V residues 244−326 of β_2GPI (Protein Data Bank entry 1C1Z) was derived from computer docking studies with the program DOCK (*34*) using a molecular docking algorithm. While domain V was kept fixed, the DMPS molecule was allowed to find the position of lowest binding energy. DMPS has to be used instead of CL for reasons of simplicity. The model is intended to give an idea about the preferential location of a single lipid molecule as modeling of a lipid assembly would be too complex.

RESULTS

Binding of β_2GPI to CL Vesicles Assessed by the Intrinsic Trp Fluorescence. Due to the different classes of tryptophan residues (four Trp residues embedded in the hydrophobic interior and one, namely, Trp316, surface-exposed), we could in general observe a very broad tryptophan emission spectrum with a maximum centered around 351 nm (top of Figure 2). It has to be mentioned that we used freshly dissolved β_2GPI and that the Trp signal was very sensitive to prolonged storage of β_2GPI in solution. For this case, we observed the emission maximum at a lower wavelength, which is an indication of protein aggregation, denaturation, or self-association processes (*35*). Upon addition of increasing amounts of CL vesicles to β_2GPI, a significant blue shift of the β_2GPI fluorescence emission maximum from 351 to 336 nm was observed (Figure 2).

Figure 3A shows this shift as a function of the lipid-to-protein molar ratio. It can be seen that the maximal amplitude of the blue shift is obtained at a low CL:β_2GPI molar ratio

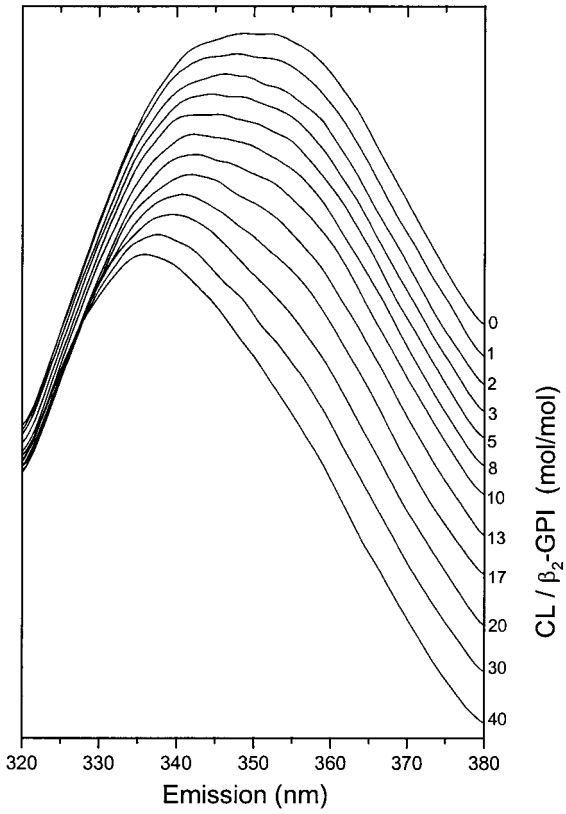

FIGURE 2: Fluorescence emission spectra of β_2GPI with increasing CL concentrations. The excitation wavelength was 292 nm. The β_2GPI concentration was 1.1 μM. Titration experiments were performed by adding small aliquots of CL LUVs. The CL concentration was varied in the ratio of 0−40 mol of CL/mol of β_2GPI. The temperature of the cuvette was maintained at 25 °C, and the measurements were acquired after equilibration for 10 min. The results are presented in a waterfall graph.

of 1:1. A further increase in the CL concentration (2−20 mol of CL/mol of β_2GPI) led to a linear decrease in the emission maximum terminating in a plateau region for CL concentrations of >20 mol. Note the experiment was accompanied by an increasing turbidity of the solution. To ensure that the procedure for titration of CL vesicles into β_2GPI solutions, which may result in initial high local concentrations of CL vesicles in the cuvette, did not influence the results presented above, single, separate mixtures were prepared (see Materials and Methods). But no differences were observed comparing titration and single-sample procedures (data not shown).

Effects of Lipid Binding on Anisotropy and Fluorescence Intensity. To assess whether β_2GPI sticks to the CL bilayer membrane, we measured the changes in fluorescence anisotropy of Trp residues at different phospholipid concentrations (Figure 3B). We found that addition of CL to β_2GPI induces a dramatic increase in the fluorescence anisotropy which reflects a decrease in the mobility of the Trp residues after binding to the CL bilayer. Furthermore, we observed a decrease in emission intensity with increasing CL concentration (Figure 3C). In contrast, the addition of neutral DMPC LUVs did not alter the emission maximum (Figure 3A), the anisotropy (Figure 3B), or the intensity (Figure 3C) of β_2-GPI even at higher lipid ratios of 80 mol of DMPC/mol of β_2GPI, confirming that negatively charged lipids are essential for the interaction of β_2GPI with phospholipid membranes.

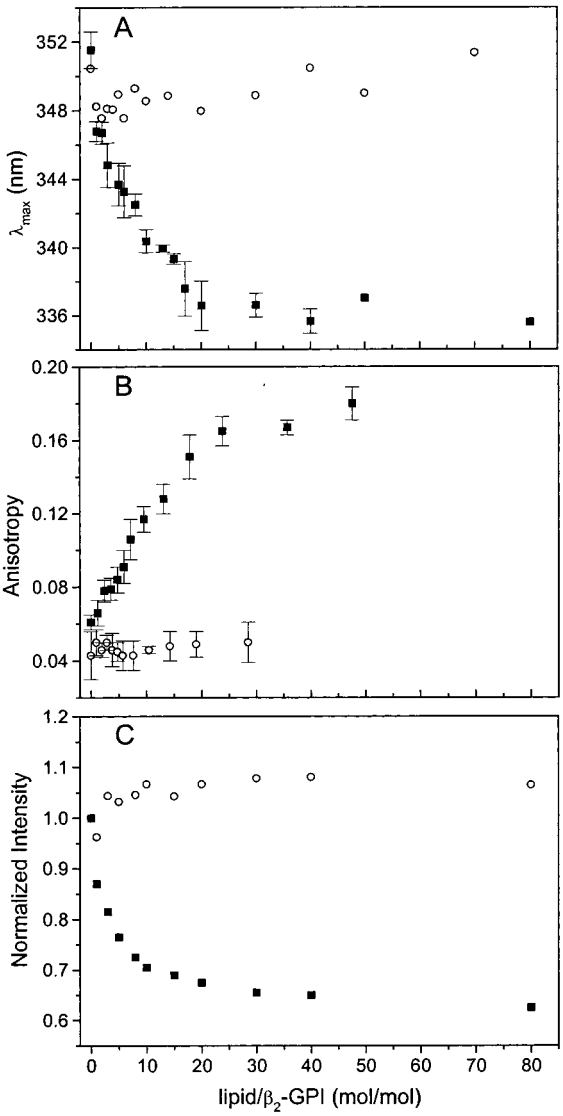

FIGURE 3: Effect of increasing lipid concentrations on the environment of Trp residues. (A) A blue shift of the emission maximum from 351 to 336 nm was observed upon addition of CL vesicles (■). Titration experiments performed with LUVs composed of neutral lipids such as DMPC (○) had almost no effect. The excitation wavelength was 292 nm. The β_2GPI concentration was 1.1 μM. The lipid concentration was varied between 0 and 88 μM (0−80 mol of lipid/mol of β_2GPI). Data represent the mean (n = 2) or the mean ± SD (n = 3). (B) Increase in anisotropy upon addition of CL LUVs (■) in comparison to addition of DMPC LUVs (○). The excitation and emission wavelengths were set to 292 and 351 nm, respectively. The β_2GPI concentration was 1.1 μM. The lipid concentration was varied between 0 and 52 μM. The values for the anisotropy were taken as the mean ± SD of 20 values from one titration experiment. (C) Decrease in the normalized intensity observed with increasing CL concentrations (■). DMPC (○) had almost no effect. The excitation wavelength was set to 270 nm. The β_2GPI concentration was 1.1 μM. The lipid concentration was varied between 0 and 88 μM. The data represent the mean of two independent measurements.

Accessibility to Water-Soluble Quenchers. To assess the exposition of Trp residues to the aqueous environment before and after binding to CL LUVs, we have chosen the water-soluble quencher acrylamide, an efficient neutral quencher of indole derivatives. The modified Stern−Volmer quenching constant K_a was determined according to eq 3 as shown in Figure 4A. We found that K_a decreased from 15.9 M^{-1} for β_2GPI in the absence of CL to 4.2 M^{-1} for a CL:β_2GPI molar ratio of 20. The decrease in K_a indicates that during CL binding the Trp residues become less accessible to the quencher. The f_a value was in both cases ~0.7. A value of 0.7 for f_a indicates that the main contribution to the steady-state emission spectrum comes from the accessible tryptophan. Further evidence for different accessibilities of Trp to the quencher is derived from the following effects. First, that acrylamide induces a blue shift of 10 nm in the emission spectrum. Second, the Stern−Volmer plot of $I_0 - I$ versus [Q] displays a downward curvature and is dependent on the wavelength (data not shown).

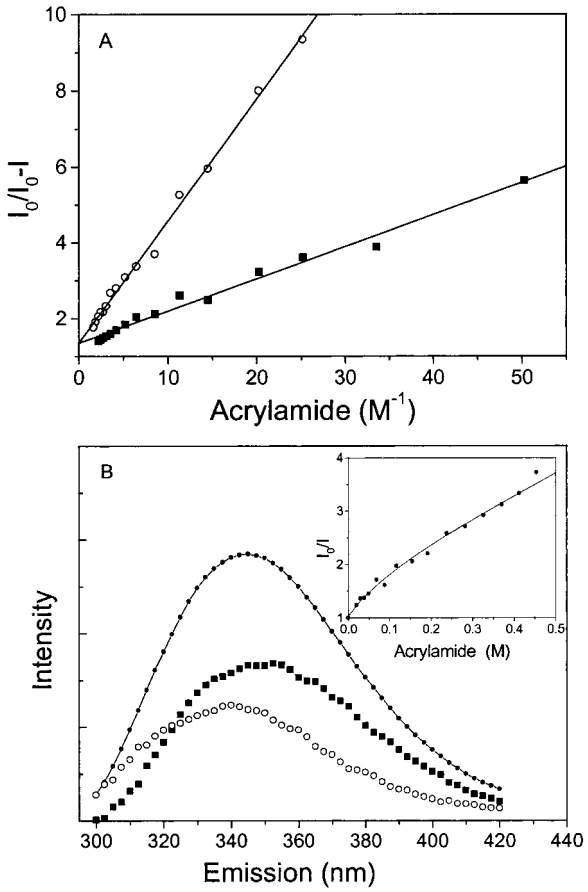

FIGURE 4: Acrylamide quenching of the β_2GPI intrinsic Trp fluorescence. (A) The modified Stern−Volmer plot for the tryptophan fluorescence quenching of β_2GPI [(■) β_2GPI in the absence of CL LUVs and (○) β_2GPI in the presence of CL LUVs] by acrylamide is shown. The β_2GPI concentration was 1.1 μM. The CL:β_2GPI molar ratio was preset to 20 mol/mol. The acrylamide concentration was varied between 0.02 and 0.6 M. (B) Quenching-resolved emission spectra of native β_2GPI. The quenching data were analyzed in terms of two components with a constant K_1 value for the accessible component (■) of 15.9 M^{-1}. The K_2 value for the inaccessible component (○) was varied between 0.6 and 3.0 M^{-1}. The steady-state emission spectrum is shown with black circles (●). The inset shows as an example the experimental points obtained for β_2GPI quenching observed at an emission wavelength of 340 nm (●). The least-squares fit of these points (−) yielded the following parameters: K_1 = 15.9 M^{-1}, K_2 = 1.7 M^{-1}, f_1 = 0.65, and f_2 = 0.35.

Selective quenching of tryptophan residues in proteins can be used to resolve the emission spectra in terms of quenched and unquenched components (*36*, *37*). The basic idea is to perform a least-squares fit of the quenching data to recover the quenching constant and fractional intensity for each wavelength (λ),

$$\frac{I(\lambda)}{I_0(\lambda)} = \sum_i \frac{f_i(\lambda)}{1 + K_i(\lambda)[Q]} \quad (4)$$

where $f_i(\lambda)$ is the fractional contribution of the *i*th tryptophan residue to the emission intensity at wavelength λ and K_i is the Stern−Volmer quencher constant of the *i*th species at wavelength λ. The quenching data were analyzed in terms of two components. The K_1 value was set to 15.9 M^{-1}, the value obtained with the modified Stern−Volmer analysis, and the K_2 value was varied between 0.6 and 3.0 M^{-1} for different wavelengths. The $f_1(\lambda)$ and $f_2(\lambda)$ values are also variable for each wavelength under the condition $f_1(\lambda) + f_2(\lambda) = 1$. Figure 4B shows the quenching-resolved emission spectra of native β_2GPI, in which the blue-shifted spectrum with a maximum at 340 nm corresponds to the almost inaccessible tryptophan residues and the red-shifted spectrum with a maximum at 351 nm corresponds to the accessible tryptophan residue Trp316. These individual emission spectra indicate that the main contribution to the β_2GPI steady-state emission comes from Trp316 with the maximum at 351 nm which is in good agreement with the results obtained from the modified Stern−Volmer analysis.

Membrane Penetration. To assess whether β_2GPI penetrates into the phospholipid vesicles, ESR spectroscopy was performed. Via this process, information about the dynamics and rotational disorder of the spin-labeled lipid molecules was gained. The spectra obtained for the 5-CL-spin-labeled vesicles, where the active group is located near the polar−apolar lipid interface, exhibited an axially anisotropic line shape which is characteristic of such labels in a fluid lipid membrane (*38*). In the presence of β_2GPI, we observed an increase in the outer hyperfine splittings ($2A_{max}$) and a decrease in the inner hyperfine splittings ($2A_{min}$) typical for a motional restriction. For 12-CL, where the active group is located closer to the terminal methyl region of the acyl chain, somewhere deeper in the phospholipid membrane, no changes in $2A_{max}$ and $2A_{min}$ could be observed (Table 1). These results indicate that protein perturbation is limited to the outer region of the membrane to which β_2GPI may anchor in the interfacial phospholipid headgroup region with the flexible loop between amino acids 313 and 316 in domain V.

Thermal Unfolding of β_2GPI. The thermal stabilities of native β_2GPI and complexes of β_2GPI with CL were examined by microcalorimetry. The heat denaturation experiments revealed no significant dependence of T_m on protein concentration and scan rate. Native β_2GPI exhibited a two-state transition with a T_m of 63.5 ± 0.1 °C and a total change in enthalpy ΔH_{cal} of 172 ± 12 kcal/mol (mean of three independent preparations of β_2GPI). When β_2GPI was reheated, the transition enthalpy decreased markedly and the $\Delta H_{vH}/\Delta H_{cal}$ ratio changed from 1 to 1.7, which is indicative of intermolecular interactions such as changes in the state of oligomerization (*39*). For a low lipid-to-protein molar ratio (1:1), the thermal unfolding behavior was very similar to that of native β_2GPI. For higher lipid ratios, i.e., 20:1 CL/β_2GPI mixtures, the DSC endotherms revealed a rather complex behavior. We found a splitting of the transition peak with maxima occurring at significantly reduced temperatures. A fit for two independent cooperative transitions revealed T_m values of ~47.5 and ~54.0 °C. The observed total enthalpy value was ~50% of the enthalpy found for native β_2GPI. It has to be mentioned that the splitting of the endotherms in the presence of CL was not exactly reproducible in terms of enthalpic contributions between different protein preparations. However, we never found a contribution of the high-temperature transition around 63 °C, suggesting that all β_2GPI molecules are associated with lipids. Rescanning of the β_2GPI−lipid complex yielded a single transition, but with a markedly reduced T_m of 52.8 °C, a ΔH_{cal} of ~100 kcal/mol, and a $\Delta H_{vH}/\Delta H_{cal}$ of >1 (Figure 5). It is conceivable that the drastic reduction in both enthalpy and T_m is the consequence of an intermediate, metastable protein association which finally results in a different aggregation state of β_2GPI in complexes with CL.

Table 1: ESR Parameters for Spin-Labeled CL Vesicles at Different Lipid:β_2GPI Molar Ratios

lipid:β_2GPI molar ratio	5-CL		12-CL	
	$2A_{max}$[a] (G)	$2A_{min}$[b] (G)	$2A_{max}$ (G)	$2A_{min}$ (G)
no β_2GPI	50.2	19.3	33.4	21.0
20:1	52.2	18.6	33.5	20.8
50:1	53.9	18.3	33.6	20.6

[a] Outer hyperfine splittings in Gauss measured at 20 °C. [b] Inner hyperfine splittings in Gauss measured at 20 °C.

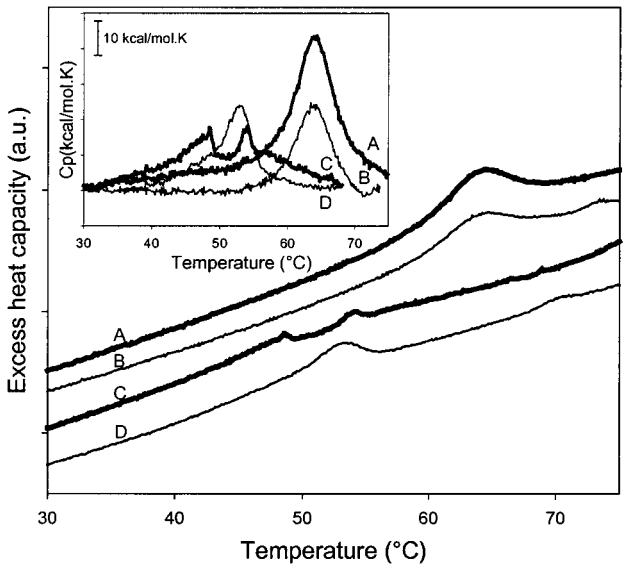

FIGURE 5: Thermal unfolding of β_2GPI and of complexes with CL vesicles. DSC thermograms were performed at a scan rate of 60 °C/h. The buffer curves were subtracted. Traces A and B depict data for the first and second scans for native β_2GPI, respectively. Traces C and D depict data for the first and second scans for CL:β_2GPI molar ratios of 20:1, respectively. The inset shows the excess heat capacity vs temperature functions after normalization for protein concentration and scan rate and baseline subtracted.

X-ray Small- and Wide-Angle Scattering. Upon addition of β_2GPI, the opalescent dispersions of CL vesicles became turbid, indicating at least partial conversion into a phase different from pure lipid or protein systems. To address this possibility, we performed X-ray scattering studies. Pure CL LUVs exhibited an X-ray small-angle scattering profile typical for single-bilayer particles, whereas the protein exhibited a characteristic particle scattering profile. The computed pair distance distribution functions $p(r)$ for CL vesicles exhibited a steep decrease toward the D_{max} value, indicating that the real maximum particle dimension is larger

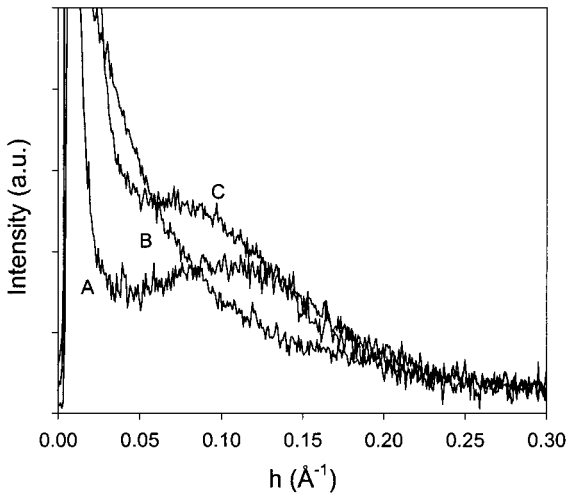

FIGURE 6: Small-angle X-ray scattering curves. Trace A shows the scattering curve of CL [4 mM CL in 10 mM Hepes buffer (pH 7.4)]. In trace B, the particle scattering curve for β_2GPI (0.2 mM) is shown. Trace C shows the scattering curve for a 20:1 lipid/protein mixture at the concentrations mentioned above. $h = 4\pi/\lambda$ (sin 2θ), where λ is the wavelength of the X-ray beam and θ the scattering angle.

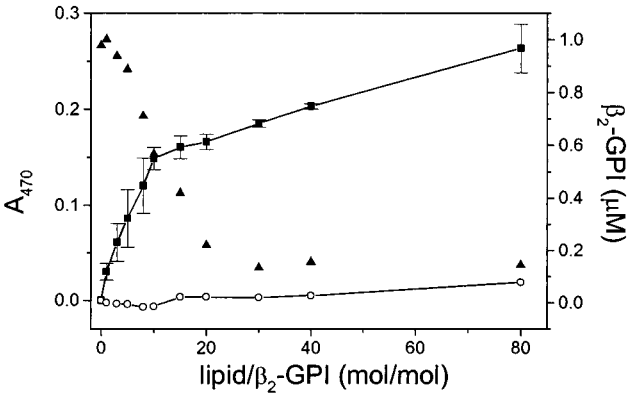

FIGURE 7: Vesicle aggregation assessed by turbidity measurements. The addition of CL LUVs (■) to β_2GPI solutions induced an increase in turbidity measured as absorbance at 470 nm (A_{470}). DMPC (○) had almost no effect. Titration experiments were performed by adding small aliquots of LUVs to the 1.1 μM β_2GPI solution. The lipid concentration was varied between 0 and 88 μM. Increasing CL concentrations (0−20 mol of CL/mol of β_2GPI) led to a steep decrease in the protein concentration measured in the supernatant (▲), approaching zero at >20 mol of CL/mol of β_2-GPI.

than the 70 nm, where the computed $p(r)$ function vanishes and hence beyond the resolution limit of the optical setup used in this experiment. However, the distance of the phospholipid headgroups in the opposite monolayers was calculated from the maximum in the $pt(r)$ function as 3.6 nm. The bilayer thickness d_m was derived (5.2 ± 0.2 nm). Upon addition of β_2GPI, we could not observe any change in the packing mode of the lipid molecules; i.e., formation of a cubic or hexagonal phase as induced by the addition of divalent ions (*29*) can be excluded. Also, we could not see any multilamellar arrangement being promoted by β_2GPI. However, a shift of the maximum located at $h = 0.11$ Å^{-1} to lower angles provides evidence for an overall increase in particle size (Figure 6). The wide-angle X-ray curves showed no ordering of the hydrogen chain structure both with and without protein.

Vesicle Aggregation As Assessed by Turbidity Measurements. The addition of CL LUVs to β_2GPI solutions induced an increase in absorbance measured at 470 nm (A_{470} in Figure 7). We did not characterize the kinetics of aggregation in more detail, but on visual inspection, an increase in turbidity of the samples immediately after addition of CL vesicles was evident. As expected, increasing concentrations of CL vesicles enhanced the rate of aggregation. In parallel, we assessed the presence of β_2GPI in the aggregates by analysis of unbound protein in the supernatant. We found that increasing CL concentrations (0−20 mol of CL/mol of β_2-GPI) led to a steep decrease in the protein concentration, terminating in a plateau region (>20 mol of CL/mol of β_2-GPI) approaching the detection limit of the protein assay (inset of Figure 7).

Macroscopic Arrangement of CL Vesicles and Mixtures with β_2GPI. The aggregation behavior of β_2GPI/CL vesicles was further surveyed by light microscopy. Light microscopic images of shaken-only vesicles of CL showed a rather heterogeneous size distribution of spherical-like particles easily flowing under the coverslip. When β_2GPI was added, a clustering of the vesicles was observed as formation of compact carpet-like regions (Figure 8). Note even very low concentrations of protein (1 mol of β_2GPI/200 mol of lipid) incited heavy clustering accompanied by turbidity.

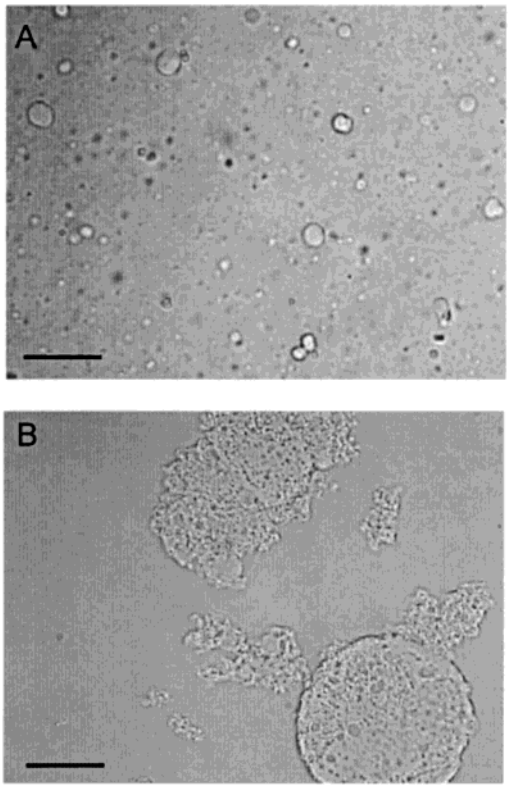

FIGURE 8: Lipid vesicle aggregation induced by β_2GPI. (A) Optical image taken with the bright field microscope on shaken-only CL vesicles (1 mM) dispersed in Tris-HCl buffer. (B) Macroscopic arrangement of the vesicles after addition of β_2GPI at a final CL: β_2GPI molar ratio of 20. The bar is 20 μm long.

DISCUSSION

Human β_2GPI is comprised of four conserved CCP modules and a distinctly folding fifth C-terminal domain. Evidence exists that the interaction of β_2GPI with acidic phospholipids occurs via domain V and is likely to be

mediated by an electrostatic interaction between a basic patch of lysine residues (C^{281}KNKEKKC^{288}) and the negative charge of the phospholipid headgroup. A closer inspection of the crystal structure of domain V would also suggest K324, K286, and K287 are only ~15 Å apart as additional coordination partners for electrostatic attractions. A putative mode of interaction between domain V and an acidic phospholipid molecule (DMPS) is more clearly illustrated in a simulation model of docking shown in Figure 1C. The simulation model further supports the idea that the flexible surface-exposed loop region composed of residues LAFW (313−316) is directly involved in membrane interaction. This is in agreement with the fact that single amino acid mutations within this motif strongly affect the phospholipid binding capacity of β_2GPI (*40*−*42*).

In this study, we have used unilamellar vesicles composed of CL as an in vitro system to mimic the assembly of β_2GPI with negatively charged phospholipids. First, we have measured the intrinsic Trp fluorescence signal of native β_2-GPI which is composed of the signals of the conserved Trp residues in CCP1−4 embedded in the hydrophobic interior of the protein backbone and the hydrophilic Trp316 in domain V (see Figure 1). The fluorescence signal was very broad with a maximum centered around 351 nm, typical for a water-exposed tryptophan residue. Intriguingly, in the fluorescence spectra reported by Wang et al. (*43*), this maximum centered around 351 nm was missing.

The resolution of our fluorescence spectrum suggests that the main contribution to the emission spectrum of native β_2-GPI comes from the Trp which is accessible to the water-soluble quencher and which according to the crystal structure has to be Trp316 in domain V. The relatively low contribution of the other Trp residues located in CCP1−4 to the fluorescence spectrum may be due to quenching by disulfide bridges (*44*) located within 4 Å of the Trp residues. Next, we probed changes in the molecular environment of the Trp residues by addition of negatively charged CL vesicles. With increasing CL concentrations, we found a blue shift in the emission maximum of ~15 nm which would coincide with the transfer of the water-exposed Trp316 to a highly lipophilic environment. This assumption is in agreement with data from moleluar modeling providing evidence for the involvement of the flexible loop region in membrane association. Further, our calorimetric results strongly support circular dichroism data demonstrating that membrane association induces conformational changes in β_2GPI (*17*, *19*, *45*). The appearance of multiple transitions for the phospholipid-associated protein suggests the existence of distinct populations of lipid−protein aggregates. The progressive association and immobilization of β_2GPI at the surface of CL vesicles likely explains the marked decline in the overall enthalpy and the reduced melting temperatures and is strongly indicative of conformational rearrangements of the protein. Thus, we assume that a destabilization of the protein and a partial loss of tertiary structural elements have taken place upon lipid association.

Now, the question of whether β_2GPI is attached to the membrane surface or penetrates into the membrane arises. We addressed the question by using spin-labeled cardiolipin molecules incorporated into CL vesicles. These labels are sensitive to changes in the lipid order depending on the depth of their location. Indeed, our ESR data showed a restriction of the side chain mobility in the outer region of the bilayer characteristic of penetration of the protein into the interfacial surface-headgroup region of the vesicles probably with the indole ring of Trp316 positioned close to the carbonyl residues. Thus, in addition to electrostatic forces, which may become weakened at high ionic strengths (*2*, *43*), our data strongly suggest that hydrophobic interactions between amino acid residues and the acyl chains of cardiolipin determine the specifity of β_2GPI for acidic phospholipid layers. Besides, our data do not support any deeper penetration into the hydrophobic membrane core. However, when CL vesicles were added to β_2GPI, the visual appearance of the solution changed to a turbid dispersion, which is a strong indication of transformation of the lipid phase. As it is well-known that cardiolipin tends to form inverted hexagonal phases by addition of divalent ions or integral membrane proteins, such a phase transition seemed to be quite reasonable. Nevertheless, our SAXS data did not show any transition into a non-single-bilayer lipid phase, indicating that the internal lipid organization of the vesicles remains preserved. This fact led us to the assumption that particle aggregation may be responsible for increasing turbidity. This coincides with another very interesting effect we could observe upon addition of CL vesicles and which concerns the significant decrease in the intensity of the fluorescence signal. One might expect that proteins which display a blue shift in the emission spectrum would have a higher quantum yield which is proportional to signal intensity. In our case, the opposite was true; namely, the intensity decreased with increasing lipid concentrations. One possible explanation could be that oligomerization of β_2GPI molecules via their hydrophobic interface on domains CCP1−3 occurs. Consequently, an intercalation of amino acid side chains could lead to a quenching of tryptophan by nearby lysine (*46*, *47*) and arginine residues (*48*) which is a common phenomenon in highly folded proteins.

Different hypotheses for the interaction of β_2GPI with membranes and aPLAs are discussed in the literature. One very interesting aspect outlines that the targets of β_2GPI are cell surface receptor proteins rather than lipids (*10*). The underlying mechanisms for such a β_2GPI−protein binding might be quite different from the association with lipids and certainly require further structural characterization. In addition, evidence exists that β_2GPI directly interacts with acidic cellular phospholipids. Some studies stress that binding of β_2GPI to negatively charged phospholipids alters the conformation of the protein, thus exposing autoepitopes (*49*); others advocate that dimerization or clustering of β_2GPI (*50*, *51*) is essential for bivalent binding of aPLAs (*21*, *52*), and only recently was it shown that dimeric chimers of β_2GPI have a much higher affinity for phospholipids (*53*). Taken together, most of these hypotheses concerning lipid association are supported well by our data. On the basis of several complementary lines of evidence, we can say that the protein is anchored in the lipid membrane interface through domain V, whereas the CCP domains probably due to the flexibility of their interdomain linkages may cross-react with other protein molecules. This is consistent with a change in protein conformation and an intercalation of amino acid side chains, in the course of which cryptic epitopes may become surface-exposed. Subsequently, intermolecular associations occur, and the macroscopic arrangement of the phospholipid−

protein complex is altered as determined by absorbance and light microscopy; on the other hand, the lipid phase behavior of the vesicles is preserved. It therefore seems likely that a structural reorientation ensuing after the initial lipid association may also exert an enhanced and modified biological affinity in vivo. At least under our experimental conditions, β_2GP facilitates molecular links which may also be a relevant feature for the in vivo autoimmune response and phagocytosis, e.g., through linkage of apoptotic cells to macrophages. Moreover, our data may be suitable for interpreting the specificity of autoantibodies to β_2GPI−CL complexes and for modeling the interaction of monoclonal antibodies with β_2GPI−phospholipid aggregates.

ACKNOWLEDGMENT

We thank Monika Zechner and Margit Eichholzer for excellent technical assistance.

REFERENCES

1. Polz, E., and Kostner, G. M. (1979) *FEBS Lett. 102*, 183−186.
2. Wurm, H. (1984) *Int. J. Biochem. 16*, 511−515.
3. Brighton, T. A., Hogg, P. J., Dai, Y. P., Murray, B. H., Chong, B. H., and Chesterman, C. N. (1996) *Br. J. Haematol. 93*, 185−194.
4. Schousboe, I. (1985) *Blood 66*, 1086−1091.
5. Nimpf, J., Bevers, E. M., Bomans, P. H., Till, U., Wurm, H., Kostner, G. M., and Zwaal, R. F. (1986) *Biochim. Biophys. Acta 884*, 142−149.
6. Nimpf, J., Kostner, G. M., and Wurm, H. (1987) *Atherosclerosis 63*, 109−114.
7. Shi, W., Chong, B. H., Hogg, P. J., and Chesterman, C. N. (1993) *Thromb. Haemostasis 70*, 342−345.
8. Field, S. L., Brighton, T. A., McNeil, H. P., and Chesterman, C. N. (1999) *Bailliere's Best Practice and Research in Clinical Haematology 12*, 407−422.
9. Delpapa, N., Sheng, Y. H., Raschi, E., Kandiah, D. A., Tincani, A., Khamashta, M. A., Atsumi, T., Hughes, G. R. V., Ichikawa, K., Koike, T., Balestrieri, G., Krilis, S. A., and Meroni, P. L. (1998) *J. Immunol. 160*, 5572−5578.
10. Ma, K. Y., Simantov, R., Zhang, J. C., Silverstein, R., Hajjar, K. A., and Mccrae, K. R. (2000) *J. Biol. Chem. 275*, 15541−15548.
11. Balasubramanian, K., and Schroit, A. J. (1998) *J. Biol. Chem. 273*, 29272−29277.
12. Chonn, A., Semple, S. C., and Cullis, P. R. (1995) *J. Biol. Chem. 270*, 25845−25849.
13. Balasubramanian, K., Chandra, J., and Schroit, A. J. (1997) *J. Biol. Chem. 272*, 31113−31117.
14. McNeil, H. P., Simpson, R. J., Chesterman, C. N., and Krilis, S. A. (1990) *Proc. Natl. Acad. Sci. U.S.A. 87*, 4120−4124.
15. Koike, T., Ichikawa, K., Kasahara, H., Atsumi, T., Tsutsumi, A., and Matsuura, E. (1998) *Lupus 7* (Suppl. 2), S14−S17.
16. Wagenknecht, D. R., and McIntyre, J. A. (1993) *Thromb. Haemostasis 69*, 361−365.
17. Borchman, D., Harris, E. N., Pierangeli, S. S., and Lamba, O. P. (1995) *Clin. Exp. Immunol. 102*, 373−378.
18. Keil, L. B., Galazka, M., el Kadi, H. S., Erickson, E. N., Jr., and Debari, V. A. (1995) *Biotechnol. Appl. Biochem. 22*, 305−313.
19. Wang, S. X., Sun, Y. T., and Sui, S. F. (2000) *Biochem. J. 348*, 103−106.
20. Roubey, R. A. S. (1994) *Blood 84*, 2854−2867.
21. Roubey, R. A. S., Eisenberg, R. A., Harper, M. F., and Winfield, J. B. (1995) *J. Immunol. 155*, 954−960.
22. Bouma, B., de Groot, P. G., van Den Elsen, J. M., Ravelli, R. B., Schouten, A., Simmelink, M. J., Derksen, R. H., Kroon, J., and Gros, P. (1999) *EMBO J. 18*, 5166−5174.
23. Schwarzenbacher, R., Zeth, K., Diederichs, K., Gries, A., Kostner, G. M., Laggner, P., and Prassl, R. (1999) *EMBO J. 18*, 6228−6239.
24. Gries, A., Nimpf, J., Wurm, H., Kostner, G. M., and Kenner, T. (1989) *Biochem. J. 260*, 531−534.
25. Bartlett, G. R. (1959) *J. Biol. Chem. 234*, 466−468.
26. Eisinger, J. (1969) *Biochemistry 8*, 3902−3908.
27. Lakowicz, J. R. (1999) *Principles of Fluorescence Spectroscopy*, 2nd ed., Kluwer Academic/Plenum Publishers, New York.
28. Ladokhin, A. S., Jayasinghe, S., and White, S. H. (2000) *Anal. Biochem. 285*, 235−245.
29. De Kruijff, B., Verkleij, A. J., Leunissen-Bijvelt, J., Van Echteld, C. J., Hille, J., and Rijnbout, H. (1982) *Biochim. Biophys. Acta 693*, 1−12.
30. Calhoun, D. B., Vanderkooi, J. M., and Englander, S. W. (1983) *Biochemistry 22*, 1533−1539.
31. Privalov, P. L. (1980) *Pure Appl. Chem. 52*, 479−497.
32. Cable, M. B., Jacobus, J., and Powell, G. L. (1978) *Proc. Natl. Acad. Sci. U.S.A. 75*, 1227−1231.
33. Glatter, O. (1977) *J. Appl. Crystallogr. 10*, 415−421.
34. Gschwend, D. A., and Kuntz, I. D. (1996) *J. Comput.-Aided Mol. Des. 10*, 123−132.
35. Pajot, P. (1976) *Eur. J. Biochem. 63*, 263−269.
36. Wasylewski, Z., Kaszycki, P., Guz, A., and Stryjewski, W. (1988) *Eur. J. Biochem. 178*, 471−476.
37. Stryjewski, W., and Wasylewski, Z. (1986) *Eur. J. Biochem. 158*, 547−553.
38. Cheneval, D., Carafoli, E., Powell, G. L., and Marsh, D. (1989) *Eur. J. Biochem. 186*, 415−419.
39. Sturtevant, J. M. (1987) *Annu. Rev. Phys. Chem. 38*, 463−688.
40. Sanghera, D. K., Wagenknecht, D. R., McIntyre, J. A., and Kamboh, M. I. (1997) *Hum. Mol. Genet. 6*, 311−316.
41. Horbach, D. A., Vanoort, E., Tempelman, M. J., Derksen, R. H. W. M., and Degroot, P. G. (1998) *Thromb. Haemostasis 80*, 791−797.
42. Mehdi, H., Naqvi, A., and Kamboh, M. I. (2000) *Eur. J. Biochem. 267*, 1770−1776.
43. Wang, S. X., Cai, G. P., and Sui, S. F. (1999) *Biochemistry 38*, 9477−9484.
44. Cowgill, R. W. (1967) *Biochim. Biophys. Acta 140*, 552−554.
45. Rauch, J., Subang, R., D'agnillo, P., Koh, J. S., and Levine, J. S. (2000) *J. Autoimmun. 15*, 231−235.
46. Sanyal, G., Kim, E., Thompson, F. M., and Brady, E. K. (1989) *Biochem. Biophys. Res. Commun. 165*, 772−781.
47. Hennecke, J., Sillen, A., Huber-Wunderlich, M., Engelborghs, Y., and Glockshuber, R. (1997) *Biochemistry 36*, 6391−6400.
48. Clark, P. L., Liu, Z. P., Zhang, J., and Gierasch, L. M. (1996) *Protein Sci. 5*, 1108−1117.
49. Matsuura, E., Inagaki, J., Kasahara, H., Yamamoto, D., Atsumi, T., Kobayashi, K., Kaihara, K., Zhao, D., Ichikawa, K., Tsutsumi, A., Yasuda, T., Triplett, D. A., and Koike, T. (2000) *Int. Immunol. 12*, 1183−1192.
50. Sheng, Y. H., Kandiah, D. A., and Krilis, S. A. (1998) *J. Immunol. 161*, 2038−2043.
51. Galazka, M., Tang, M., Debari, V. A., Kohles, J. D., Lee, J. K., Keil, L. B., and Petersheim, M. (1999) *Appl. Biochem. Biotechnol. 76*, 1−13.
52. Willems, G. M., Janssen, M. P., Pelsers, M. A. L., Comfurius, P., Galli, M., Zwaal, R. F. A., and Bevers, E. M. (1996) *Biochemistry 35*, 13833−13842.
53. Lutters, B. C., Meijers, J. C., Derksen, R. H., Arnout, J., and de Groot, P. G. (2001) *J. Biol. Chem. 276*, 3060−3067.

BI0114372